brain sciences

MDPI

Article

Therapeutic potential of focused ultrasound for Alzheimer's Disease pathology depends on ultrasound dose and age, in vivo.

Alissa Phutirat [1], Kahte A. Culevski[1], Hannah Mach[1], Jamie Kwon[1], Henry Tan[1], Gabe Koh[1], Caren Marzban[2], Pierre D. Mourad[1,3,*]

[1] Department of Neurological Surgery, University of Washington, Seattle WA
[2] Applied Physics Laboratory, University of Washington, Seattle WA.
[3] Division of Engineering and Mathematics, University of Washington, Bothell WA
* Correspondence (PDM): doumitt@uw.edu

Abstract

Background/Objectives: Alzheimer's Disease (AD) and vascular dementia contribute up to ~75% of dementia cases, determined via autopsy. AD arises in part due to the buildup of aberrant proteins (amyloid beta - Aβ, tau); vascular dementia is caused by reduced cerebral blood flow. Each damages brain. Bobola et al [21] found that their focused ultrasound (FUS) protocol applied to the brains of the 5XFAD mouse model of AD reduced their Aβ by 50% through activation of microglia. Eguchi et al [23] found that their own FUS protocol applied to the brains of the same mouse model reduced Aβ by 15% and increased cerebral blood flow by 50% through an increase in endothelial nitric oxide synthase (eNOS). Here we sought to test the effectiveness of a combined version of those two FUS protocols, expecting both a decrease in Aβ burden and an increase in eNOS.

Methods: Using a diagnostic ultrasound probe, we applied our combined FUS protocol to the left hippocampus of anesthetized 5XFAD mice, for an hour a day, for three days for young mice and for five days for old mice. On day three or five, respectively, we harvested their brains and performed histological analysis to assess Aβ burden, microglial activation and their co-localization with Aβ, and the burden of eNOS within neuronal nuclei and outside of neurons.

Results: Relative to untreated mice, the treated young mice had more activated microglia co-located with Aβ, reduced Aβ burden, with no change in each measure of eNOS. In contrast, the treated old AD mice had no change in activated microglia co-located with Aβ, and no change in Aβ burden. However, relative to untreated old AD mice, FUS *decreased* extra-neuronal eNOS and *increased* intra-neuronal / intra-nuclear eNOS.

Conclusions: The ability of our FUS protocol to reduce Aβ burden and alter the eNOS distribution depend critically upon the age of the AD mice, at least in part because of substantial differences in amount of microglia available to attack the amount of Aβ plaque versus age. The observed decrease in extra-neuronal eNOS distribution for the older AD mice raises the concern that our protocol will increase ischemia while the increase in intra-neuronal eNOS may at least in part counteract that effect. These findings identify a therapeutic window for FUS as applied to AD; it suggests that earlier intervention may

Academic Editor: Firstname Lastname

Received: date
Revised: date
Accepted: date
Published: date

Citation: To be added by editorial staff during production.

maximize Aβ plaque removal while eNOS modulation in older mice warrants further investigation to mitigate potential ischemic risks.

Keywords: Alzheimer's Disease; Vascular Dementia; focused ultrasound; FUS.

1. Introduction

Dementia is a class of devastating neurodegenerative disorders with a huge personal and societal burden [1]. A prominent form known as Alzheimer's Disease (AD) is characterized histologically by the accumulation of amyloid-β (Aβ) plaques and phosphorylated tau tangles (p-tau) – [2,3,4]–- and clinically by profound cognitive decline, progressive memory loss, and early mortality [5]. The dominant view of AD identifies the accumulation of those aberrant proteins, especially p-tau, as playing a causal role in the progression and effects of this disease, a complex topic with a range of studies supporting or refuting that view [6]. Vascular dementia – a reduction in cerebral blood flow correlated with aging – also damages human brain in the long term [5]. Together, AD or vascular dementia, or their combination (mixed dementia), account for around 75% of dementia as determined by autopsy [5].

There exists a role for nitric oxide synthase (NOS) in each of vascular, AD, and mixed dementia. NOS expresses predominantly in endothelial cells (known as eNOS) where it helps regulate vascular tone hence cerebral blood flow. It also expresses in the nuclei of neurons, where, in the context of AD, it can maintain synoptic function during a significant percentage of progression of the disease [7]. Nonetheless, aberrant nitric oxide presence and function can contribute significantly to a variety of neurodegenerative processes, including, necrosis, apoptosis, autophagy, and neuronal death, all relevant to Alzheime''s disease pathogenesis [8,9].

Recently approved medications (Aducanumab and Lecanemab) have discernable though modest impact on the rate of cognitive decline through reduction of amyloid beta plaque burden [10]. Among the variety of therapeutic alternatives to medications, recent research has highlighted the potential of non-pharmacological approaches to reduce the burden of these aberrant proteins. Light-based stimulation of AD brain with frequencies in the gamma band, specifically 40 Hz, cleared ~50% of Aβ from the visual cortex of awake 5XFAD mice exposed to five days of one-hour sessions of 40 Hz blinking light relative to sham [11]. Subsequent work combining light and acoustic stimulation in this frequency band showed reduction of Aβ in the visual and auditory cortices, as well as the prefrontal cortex and hippocampus of 5XFAD mice [12]. This remains an area of active research [13]. Enhancing gamma activity in the brain is an *a priori* plausible approach to treating dementia because gamma oscillations participate in perception and cognitive function, with impairments in this frequency band in AD mouse models and patients (reviewed by [11]).

Focused ultrasound (FUS, sometimes called low intensity focused ultrasound – LIFU) that disrupts the blood-brain barrier (BBB) can reduce aberrant Aβ plaque burden. Leinenga and Götz [14] represents an early example of this approach, combining transcranial delivery of FUS with microbubbles, whose FUS-induced mechanical behavior disrupts the BBB. They demonstrated that four FUS sessions distributed over eight weeks reduced the Aβ plaque burden and improved the memory of a mouse model of AD. Follow-on work with the same theme includes Karakatsani et al [15], among others. Recently, Rezai et al [16] demonstrated that the same procedure applied to AD patients increased the flux of an FDA-cleared antibody against Aβ plaque, safely producing a significant reduction Aβ plaque burden relative to contralateral brain tissue not exposed to FUS. Mehta et al [17] offer a review of this topic.

FUS that does not disrupt the BBB can also improve dementia pathology and/or symptoms. The original FUS protocol without microbubbles used by Götz and colleagues did not alter AD pathology [18]. Their application of a different FUS protocol has improved AD symptoms, *in vivo,* with and without alteration of the underlying aberrant protein burden – reviewed by them in Balbi et al [19]. Human studies of FUS for dementia are emerging, such as Nicodemus et al [20]. Motivated by the 40 Hz pulsed light treatment of AD pathology cited above, Bobola et. al. [21] demonstrated comparable microglial activation acutely and comparable (~50%) and rapid (over five days) reduction in Aβ plaque, also in 5XFAD mice. They used 40 Hz pulses of transcranial, focused ultrasound without microbubbles to disrupt the BBB. Importantly, this occurred in and around the targeted hippocampus, rather than only the visual cortex as reported by [11]. Park et. al. [22] corroborated these observations and extended them, observing changes in brain connectivity and enhancement of spontaneous EEG gamma power. Yet others have taken a separate approach to reducing Aβ plaque burdens in an anesthetized 5XFAD mouse model without concurrent use of microbubbles [23]. Their FUS protocol, different than that of Bobola et. al. [21] and Park et. al. [22], causally increased total eNOS protein expression, cerebral blood flow, and reduced Aβ plaque after a three sessions per week, two-month treatment protocol.

Given the importance of pure AD, vascular dementia, and their combination, we constructed a protocol that combined the temporal patterns of each of Bobola et. al. [21] and Eguchi et. al. [23], seeking thereby to produce a combination of their biological effects in AD mouse brain. We first applied that protocol to relatively young AD mice, for three days. Those results motivated subsequent application to a substantially older cohort, for five days. The biological results depended strongly on the intervention's duration in terms of days as well as mouse age.

6. Materials and Methods

Overview of Experimental Procedures

Animal Model. We used 5XFAD (C57BL/6) transgenic mice (MMRRC stock #34840; Jackson Laboratory, Maine, USA). This model overexpresses mutant human APP(695) with the Swedish (K670 N/M671L), Florida (I716V), and London (V717I) Familial AD (FAD) mutations and human PS1 with two FAD mutations, M146L and L286V [24]. 5XFAD (C57BL/6) mice present with a significant Aβ plaque burden that emerges between 2 and 4 months of age. However, the extent of pathological (and functional) change increases as they mature [25]. For example, at 9-12 months of age, 5xFAD mice display motor and cognitive deficits compared to their wild type (WT) whereas mice 5-7 months of age do not. This difference in function between these age groups prompted us to increase the number of FUS treatments for the older mice relative to the younger mice.

We used G* power [25] and the results of Bobola et al (47 +/- 8% reduction in Aβ plaque due to FUS), along with the assumptions of alpha = 0.05 and beta = 95%, to support our use of n = 3 mice in our study.

Timeline of three-day chronic study. We treated three anesthetized young 5XFAD mice with FUS applied simultaneously to each hemisphere of their brains as described below, for one hour per day, for two days. On the third day, after re-establishing an anesthetic plane, electrocorticography (ECoG) wires were placed in the hippocampus and somatosensory cortex within each brain hemisphere to measure brain activation in response to one more hour of FUS. We then sacrificed and perfused the mice. Three sedated mice were exposed to sham FUS under the same pre/post ultrasound procedures.

Timeline of five-day chronic study. We treated three anesthetized old 5XFAD mice with FUS applied simultaneously to each hemisphere of their brains as described below, for one hour per day, for four days. On the fifth day, after re-establishing an anesthetic plane, ECoG wires were placed in the hippocampus and somatosensory cortex within each brain hemisphere to measure brain activation in response to an additional dose of FUS for one hour. We then

sacrificed and perfused the mice. Three sedated mice were exposed to sham FUS under the same pre/post ultrasound procedures.

Detail of experimental procedures

Anesthesia. After initial exposure to isoflurane at 2–3% and placement within the experimental setup (figure 1A), mice remained exposed to isoflurane at 1.5-2.5% through a nose cone to maintain sedation throughout the experiment, adjusted as necessary to keep a healthy anesthetic plane.

Experimental setup – chronic studies without ECoG. After induction of an anesthetic plane using isoflurane, we placed the treatment animal on a heating pad and into a mouse stereotaxic headpiece (Stoelting Digital Lab Standard). We then applied ophthalmic ointment (Artificial Tears; Akorn; US) to their eyes followed by a depilatory cream (Nair Hair Remover Cocoa Butter; Nair; Ewing, New Jersey, USA) to the top of the mouse head in order to remove its fur. We attached a custom, 3D-printed pointer to the distal face of the diagnostic ultrasound transducer to provide a visual cue for the focal ultrasound projected by that transducer. The pointer plus our digital stereotax guidance system (WPI, Sarasota, FL) allowed us to guide the ultrasound transducer to over the correct portion of the head of the mouse. We then placed ultrasound gel (Aquasonic 100 Ultrasonic Gel; Next Level Technology; Los Angeles, California, USA) on the dorsal portion of the mouse's head, lowered the distal face of the transducer into the gel, then applied FUS (Figure 1A). Specifically, we placed the FUS focus at 1.43 mm posterior of Bregma and 1.3 mm below the skin surface, into sections C1-C3 of the hippocampus and surrounding brain tissue.

Experimental setup – acute study with ECoG. After induction of an anesthetic plane and removing hair with Nair as above, we injected lidocaine and bupivacaine (AuroMedics Pharma; East Windsor, NJ) subcutaneously into the dorsal aspect of the mouse skull, surgically exposed the skull, then drilled holes for placement of electrodes in the motor cortex and hippocampus of each hemisphere, with coordinates determined by the Allen Institute's online mouse atlas. We created custom made ECoG electrode arrays by soldering five silver electrode wires (0.0130-inch coated/0.010-inch bare diameter) as well as one silver ground wire (0.0190-inch coated/0.015-inch bare diameter). We connected that array into a preamplifier chip itself connected to a biosignal analog converter (Pinnacle Technology, Lawrence, Kansas, USA). eCOG signals propagated from the chip into PowerLab, hence into LabChart (AD Instruments Inc; Dunedin, New Zealand) for real-time monitoring of the data and to facilitate post-hoc analysis with MATLAB (MathWorks, Inc).

Ultrasound setup and protocol. We used a Vantage™ Research Ultrasound System (Verasonics Inc; Kirkland, Washington, USA) with a P42 diagnostic ultrasound probe (Philips Ultrasound; Bothell, Washington, USA). The spatial peak pulse average (Isppa) was 90 W/cm^2 (less than half the value used by Bobola et al [21] and below diagnostic ultrasound limit on Isppa), as measured in water at a distance where it would overlap with the hippocampus (Figure 1B). Acoustic output of the Verasonics V-1 and ATL P-4 transducer were measured using an Onda HNR-500 needle hydrophone (Sunnyvale, CA). Prior to data collection, water in the scanning tank was degassed to less than 2% dissolved oxygen. A series of 1D and 2D scans were collected to characterize the acoustic sound field at low pressures and extrapolated to higher pressures. Additional measurements were made away from the focus at higher voltages to confirm linearity (pressure as a function of voltage) of the Verasonics power supply and confirm that the Verasonics could output long duration pulses as used in this study without droop. The FUS protocol (Figure 1C) combined the large-scale pulse pattern of Bobola et. al. [21] with the fine-scale pulse pattern of Eguchi et. al. [23]. This protocol used a carrier frequency of 2 MHz, pulsed 40 times/second (40 Hz PRF), each lasting for 5 milliseconds. Within each 5 millisecond-long pulse we distributed 30 bursts that each lasted for 400 microseconds, delivered at a rate of 6 kHz wave. Each session lasted one hour.

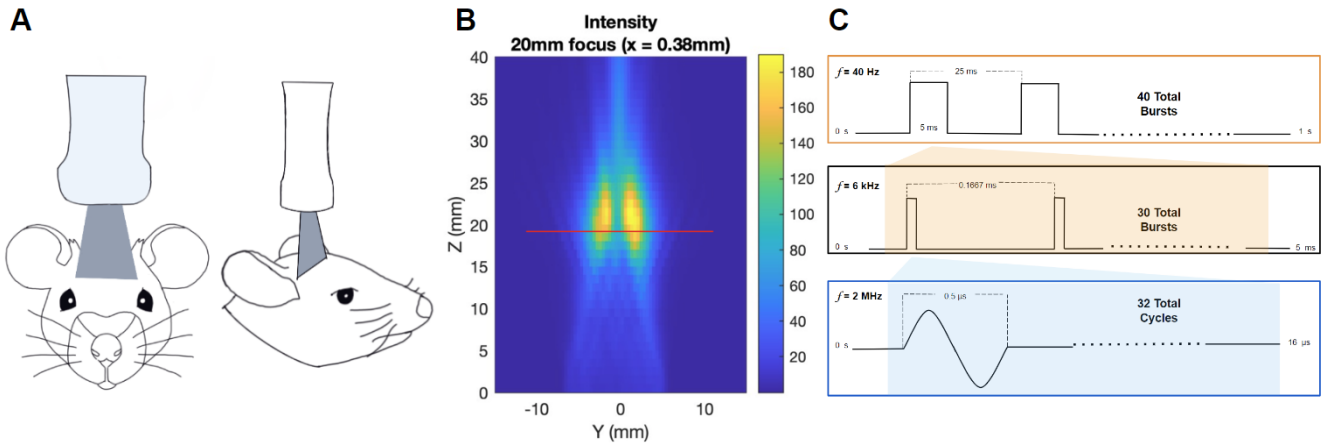

Figure 1. (A) Position of ultrasound relative to bregma on a mouse skull. **(B)** Holographic image of the FUS beam in the radial (y) plane as a function of distance from the probe face. The red line denotes where we measured the intensity value (Isppa = 90W/cm^2) in the left focus – the target of our histological analysis. **(C)** Schematic of our novel FUS Protocol.

Euthanasia and brain harvesting. Deeply anesthetized mice were immediately euthanized after the final FUS treatment using transcardiac perfusion method with formaldehyde in order to preserve brain tissue. Brains were promptly and carefully extracted from the skull and stored in formalin.

Histology. Brain tissue was processed by Fred Hutchinson Department of Histopathology. Mouse brains were fixed in NFB (neutral buffered formalin) through perfusion, trimmed to the site of ultrasound application and sent to our vendor in 70% ethanol. Samples were then processed in paraffin blocks and sliced at the region of interest in 12 serial slices per brain with two slices of tissue placed per slide. The ROI began at the center of the ultrasound focus and then proceeded rostral in consecutive slices. For the three-day chronic study, processed before the COVID-19 pandemic, each slice measured four microns in thickness. The slides were stained from the center of the US application to the rostral portion in this order: two slides with a total for four slices stained for Aβ + microglia + DAPI, two slides with a total for four slices stained for Aβ + eNOS + DAPI, two slides with a total for four slices stained for Hematoxylin and Eosin. For the five-day chronic study, processed during the COVID-19 pandemic by a different group due to loss of most skilled personnel at Fred Hutchinson, each slice measured 7-10 microns in thickness. The slides were stained from the center of the US application to the rostral portion in this order: one slide with two slices stained for Aβ, one slide with two slices stained for eNOS and Eosin.

Aβ was stained with rabbit monoclonal anti beta amyloid 1-42 antibody (Clone mOC64; Abcam, Cat. No. Ab201060). Microglia was stained with rabbit polyclonal anti-Iba1 (Wako Chem; Cat. NO. 019-19741). eNOS was stained with Rabbit anti Phospho-eNOS antibodies known to bind to activated eNOS (Online Inc Cat. No. ABIN6256115). For fluorescent imaging we stained microglia with Alexa Fluor 488 Dye, Aβ with Cy3 Dye from ThermoFisher Scientific, and nuclei with DAPI counterstain (Cat. # D1306). (As noted above: due to loss of skilled personnel during to the COVID-19 pandemic, we were able to use fluorescent imaging for brain tissue only for mice from the three-day chronic study. We had to switch to DAB staining for microglia, Aβ and eNOS plus Eosin for cell nuclei for mice for the five-day chronic study.)

Overview of Image Analysis

Image Acquisition. Images of histological tissue slides were captured at 125x magnification using ZEN microscopy software and an immunofluorescent microscope (Zeiss Axiozoom V.16; Oberkochen, Baden-Württemberg, Germany). For standardization, the eNOS channel in far red was set as the reference channel. Green and blue channels were added for detecting Aβ and nuclei, respectively. Using a range indicator, intensity of the image was adjusted, and exposures noted. Images were saved and exported as a tri-channel CZI file.

Image Analysis. We processed histopathological images using FIJI, a free image processing package within ImageJ. Images were uploaded with the most pixels to reflect the realistic dimensions of the brain slice based on length per pixel measurements. We performed our analysis within the left hemisphere of each slide, consistent with the placement of the more intense FUS focus. Using the polygon selection, the outline of the brain was traced as a region of interest (ROI). If they were visible, the ventricles were also outlined then subtracted from the larger ROI. The images were then filtered to remove possible artifacts by shape and size. This included running a macro that standardized scale of 0.93μm per pixel. We identified common structures in adjacent slices to align features of interest for subsequent analysis. All images had standardized filtering which consisted of running a "Subtract Background" with a "Rolling ball radius" of 50.0 pixels and the light option. The option "Otsu" was used to create a binary. The "Extended Particle Analyzer" from BioVoxxel Toolbox was used to analyze microglia, Aβ and nuclei. The "roundness" cut-off was specified such that the area only included particles that measured more than 706 μm^2, and the roundness was between 0.523 and 1 (Bobola et al, [14]).

Co-localization of active microglia and plaque. Both microglia and Aβ plaques were made binary and counted using the particle analyzer in FIJI where size, roundness, location, and area were obtained. Inactive microglia were characterized by their long and thin skeletal bodies whereas active microglia were characterized by their hypertrophic cell body and more retracted processes. Activated microglia in the images were formally identified as having a sufficiently 'round' structure – quantitatively identified by the roundness function with a minimum value of 0.523 as in Bobola et al [21], see also their Figure 2. Plaques that had at least one active microglia overlapping within 0.15μm were considered co-localized as in Bobola et al [21]. The percentage of plaques colocalized with microglia were calculated within each tile across a comparably sized region of interest between sham and FUS-treated mice.

Plaque Burden. After each plaque was accounted for, we created a quantile-quantile plot to determine the range of plaque sizes for which there existed a difference in population. A size range by area (in square microns - μm^2) was thus created for mice from each cohort. The percentage of plaque, including as a function of individual plaque area, was calculated within each tile across a comparably sized region of interest between sham and FUS-treated mice.

Quantile-quantile analysis. This technique determines if two data sets – one graphed along each of the horizontal and vertical axes – come from populations with a common distribution. Data points along a 45-degree line (blue in the figures) come from the same distribution. Those data points that deviate meaningfully from that 45-degree line *may* come from a different distribution, thus motivating a formal statistical test of that possibility, above versus below the crossing point of the data against that 45-degree line. The red-dotted line shown on the graph results from a linear regression through the lowest value points. MATLAB was utilized to process histological Aβ plaque data and create quantile-quantile plots. Points at which the plaque size differed between two groups were noted using MATLAB and further analyzed with a Welch two sample T-test [27].

Quantification of eNOS. The percentage area of all eNOS was calculated within each tile across a comparably sized region of interest between sham and FUS-treated mice. eNOS within nuclei of any cell were identified by its co-localization with Eosin, as appropriate. To differentiate between neuronal nuclei and the nuclei of endothelial cells, we noted differences in cell shape: neurons with many branches and complex shapes versus endothelial cells, that surround blood-vessel walls. We also noted differences in the circularity of the nuclei: nuclei in neurons are rounder than in endothelial cells. Regarding the latter point, the nuclei of neurons had reference circularity filtering of 0.80-1.0 and only eNOS that overlapped with nuclei were counted as eNOS within the neuron [28, 29].

Statistical Analysis. Since there were two brain-tissue slices per slide, we used the Welch two-sample t-test in R software to assess for any difference between sham and treated brains, for co-localization, for Aβ burden, and for eNOS distribution [27]. We plotted the results in terms of mean +/- the standard error of the data.

3. Results

3.1. Histopathology and ECoG results

Figure 2 shows sample histology for each of amyloid beta, microglia, and eNOS.

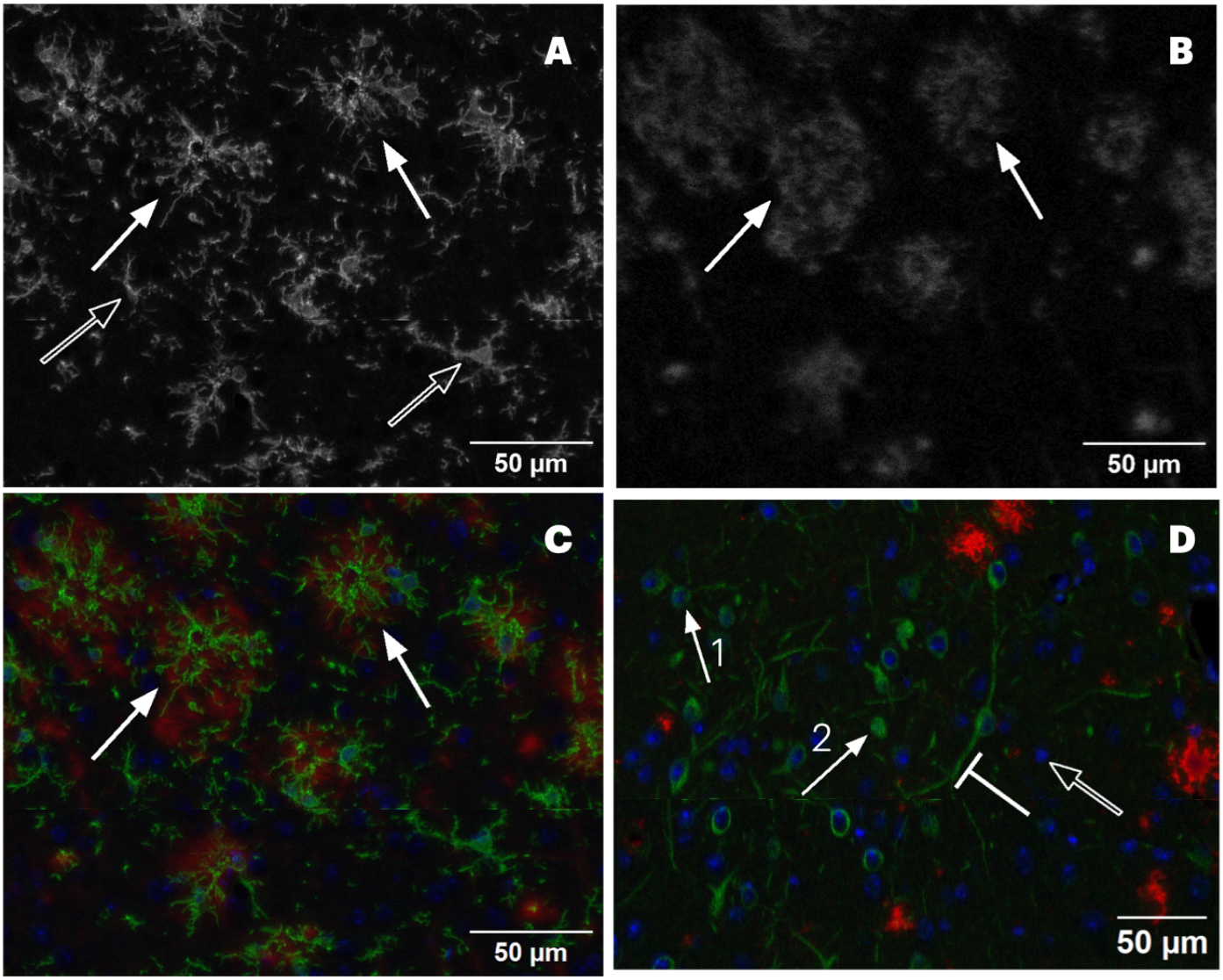

Figure 2. Representative immunofluorescent histopathology images from three-day FUS treated mice. **(A)** Microglia immunofluorescence image; closed arrows point to activated microglia; open arrows show inactivated microglia. **(B)** Closed arrows point to examples of Aβ plaque. **(C)** Superposition of microglia and Aβ plaque channels showing overlap of activated microglia and Aβ plaque. **(D)** eNOS (green), nuclei (blue), and Aβ plaque (red). Here in D, the closed arrow #1 points to eNOS within the nuclei of a neuron; the closed arrow #2 and the bar-headed arrow point to eNOS outside of the nuclei of a neuron; the open arrow points to a cell nucleus without eNOS.

Figure 3 shows representative histopathological results from the five-day chronic study.

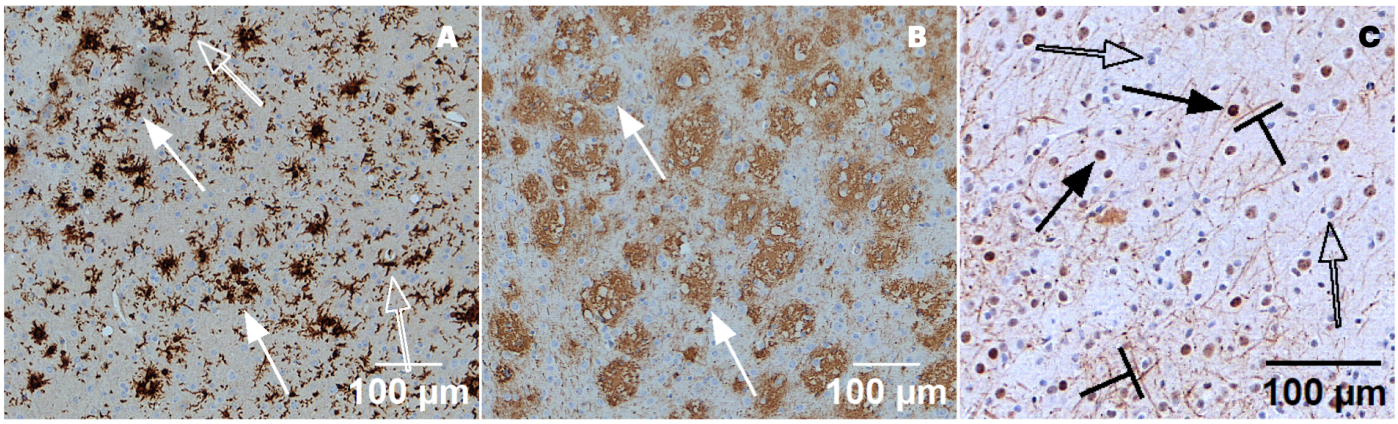

Figure 3. Representative histopathology image from five-day FUS treated mice. **(A)** Activated microglia identified with closed arrows; unactivated microglia identified with open arrows. **(B)** An image of Aβ plaque taken from a slice of brain adjacent to the one shown in figure 3A, with the closed arrows here corresponding to the closed arrows in 3A. **(C)** An image of eNOS (brown) and cell nuclei (blue). The closed arrows point to intraneuronal eNOS overlaping with round neuronal nuclei; the open arrow points to a cell nucleus without eNOS; the bar-headed arrows show eNOS outside of nuclei.

Finally, our ECoG measurements recapitualted our earlier results (Bobola et al [21], their figure 4): we observed a strong band of 40 Hz brain activity in the left hippocampus of our treated mice (data not shown), confirming FUs-induction within brain, shown in Bobola et al [21] as necessary to activate microglia.

3.2 Analysis of plaque and eNOS burdens

3.2.1. *Results for young AD mice treated with FUS for three days.*

These mice had an average age of 7.5 +/- 0.51 months. Our quantile-quantile plot for Aβ plaque in this cohort of mice suggested that there may exist meaningful differences in plaque burden for plaque area greater than versus less than 1800μm² (Figure 4).

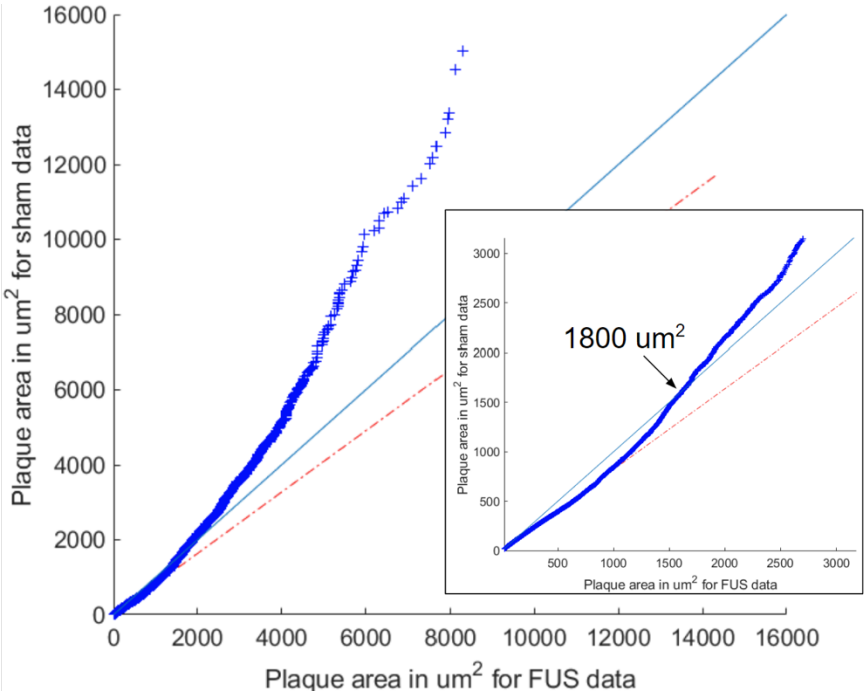

Figure 4. Quantile-quantile plot of plaque size after three days of FUS versus sham FUS treatment of young AD mice. Close up of the inflection is point shown in the bottom right corner. The blue line lies along a 45-degree angle, while the dash/dotted red line lies tangent to the lowest range of data values.

The QQ plot motivated sub-analysis of plaque burden and co-localization within those ranges. The number of plaque (scaled by total plaque number) of all sizes colocalized with active microglia in mice treated with FUS was significantly greater than for sham-treated mice (Figure 5).

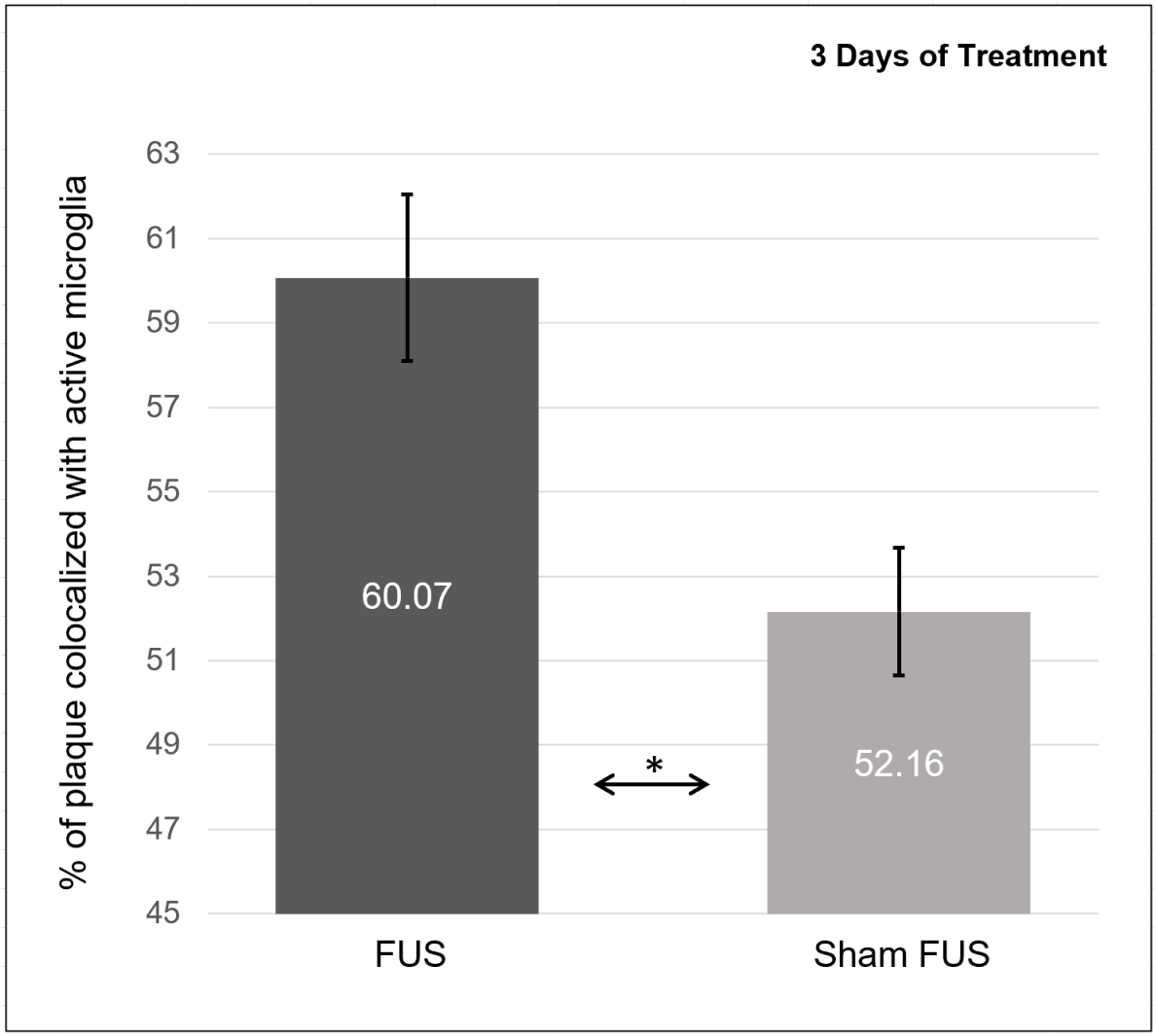

Figure 5. Co-localization of plaque with at least one active microglia in young AD mice (sham) treated with FUS for three days. Welch two-sample t test p value = 0.034. n = 3 mice with two histological samples per mouse.

The difference in the total area covered by plaque across all sizes for (sham) FUS treatment trended towards statistical significance (Fig. 6A). FUS treatment significantly reduced the percentage of brain covered by plaque with plaque sizes greater than 1800µm² (Fig. 6B) though not below 1800µm² (Fig. 6C).

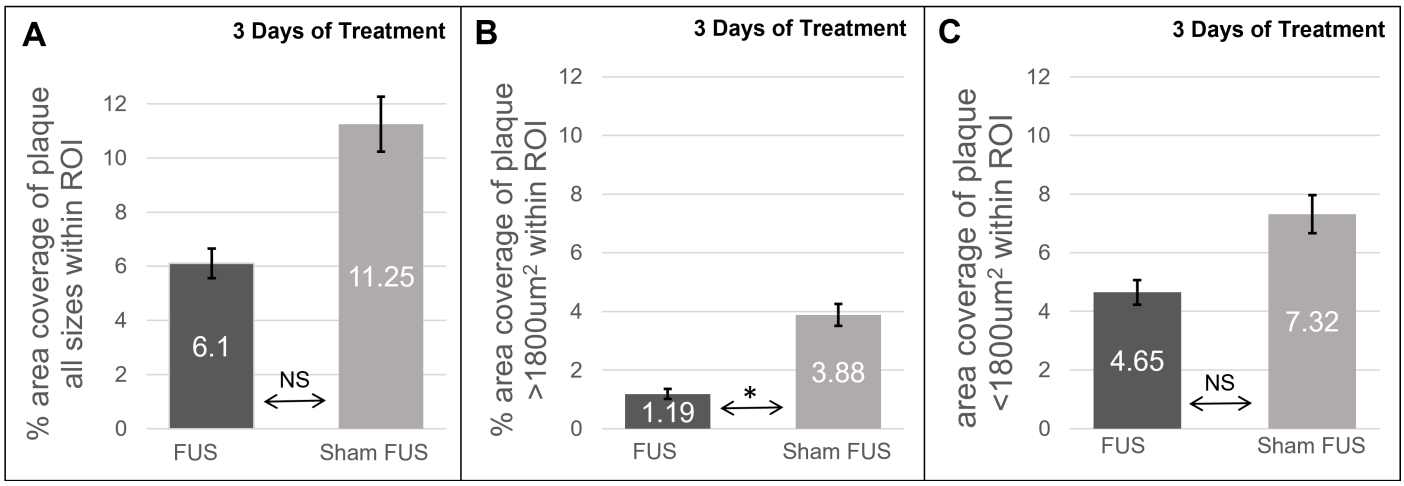

Figure 6. Plaque burden of all sizes for young AD mice (sham) treated with FUS versus sham FUS for 3 days. **(A)** For the percentage area of brain covered by plaque of all sizes, Welch two-sample t-test p value = 0.10. **(B)** For percent area coverage of plaques greater than 1800µm², p value = 0.045. **(C)** For the percentage area of brain covered by plaques of less than 1800µm², p value = 0.18. n = 3 mice with two histological samples per mouse.

The total amount of brain with eNOS showed no significant difference between sham and treated young AD mice. In addition, the distribution of eNOS inside and outside neuronal nuclei also did not demonstrate a difference (Fig. 7).

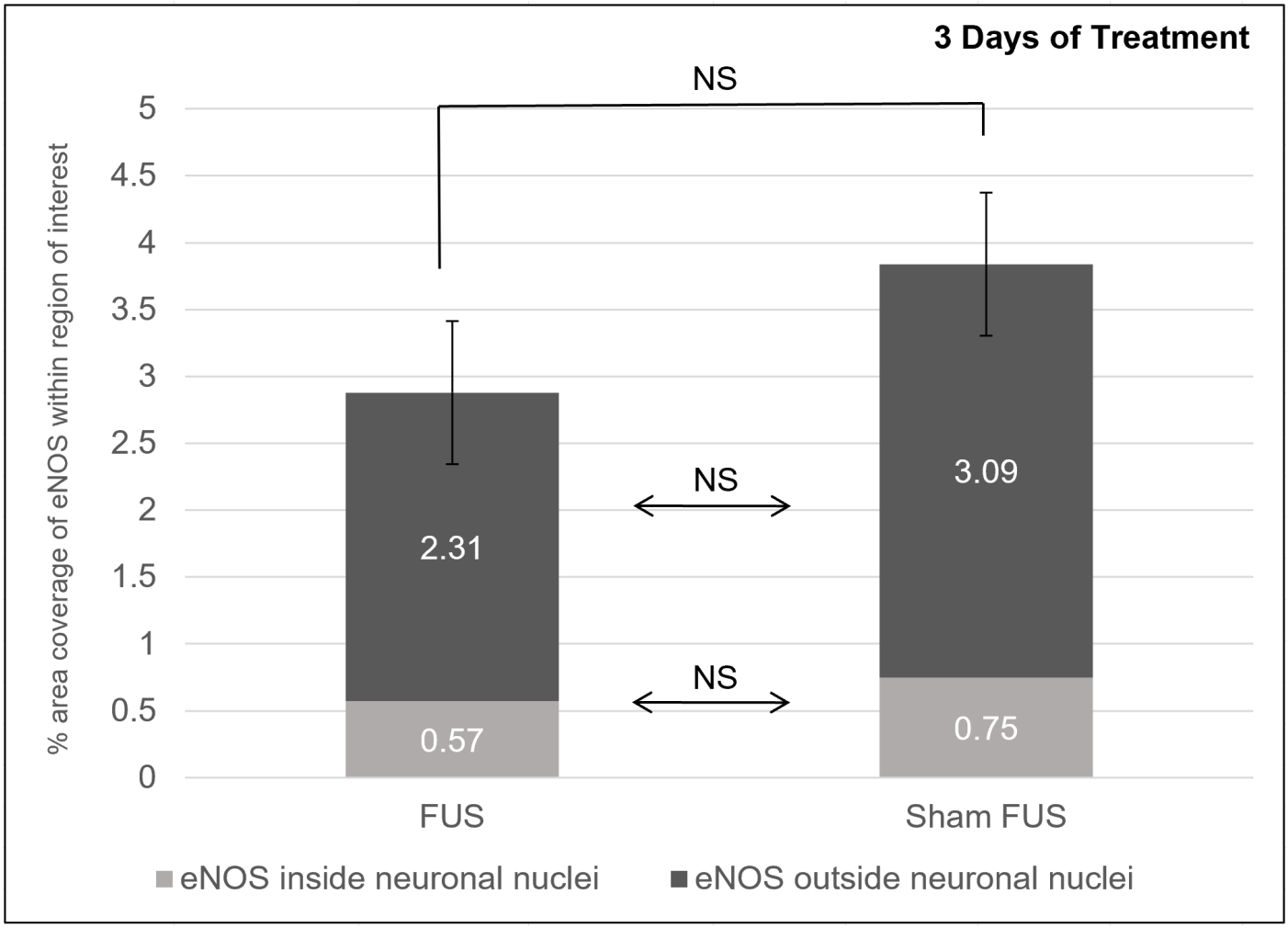

Figure 7. Distribution of eNOS within ROI of young AD mice (sham) treated for three days with FUS. Dark gray indicates eNOS outside of neuronal nuclei and light gray indicates eNOS inside neuronal nuclei. p-value of Welch two-sample t-test = 0.44 comparing percent eNOS outside neuronal nuclei. p-value of Welch two-sample t-test = 0.44 comparing percent eNOS inside neuronal nuclei. p-value for total percent area coverage of eNOS between groups = 0.59. n = 3 mice with two histological samples per mouse.

Table 1. Results for 'young' mice treated for three days with (sham) FUS. Here, * $p < 0.01$

Three days of treatment (n = 3 per group) (median +/- SE) Age 7.5 +/- 0.51 (months)			
Parameter	**FUS**		**Sham FUS**
% plaque burden	6.10 +/- 1.09		11.25 +/- 2.04
# of microglia/um^2	0.18 +/- 0.07	*	0.15 +/- 0.11
# activated microglia/um^2	0.10 +/- 0.10		0.09 +/- 0.09
% colocalized plaque	60.08 +/- 3.02	*	52.17 +/- 3.96
% area eNOS	2.89 +/- 1.07		3.71 +/- 1.03
% eNOS outside neuronal nuclei	90.16 +/- 4.77		89.63 +/- 1.27
% eNOS inside neuronal nuclei	9.84 +/- 4.77		10.37 +/- 1.27

3.2.1. *Results for old AD mice treated with FUS for five days.*

The old AD mice had an average age of 12.17 +/- 0.13 months. The quantile-quantile plot for amyloid beta plaque in this cohort of mice reflected possible differences in plaques with area greater than 3000μm^2 versus below that value (Figure 8).

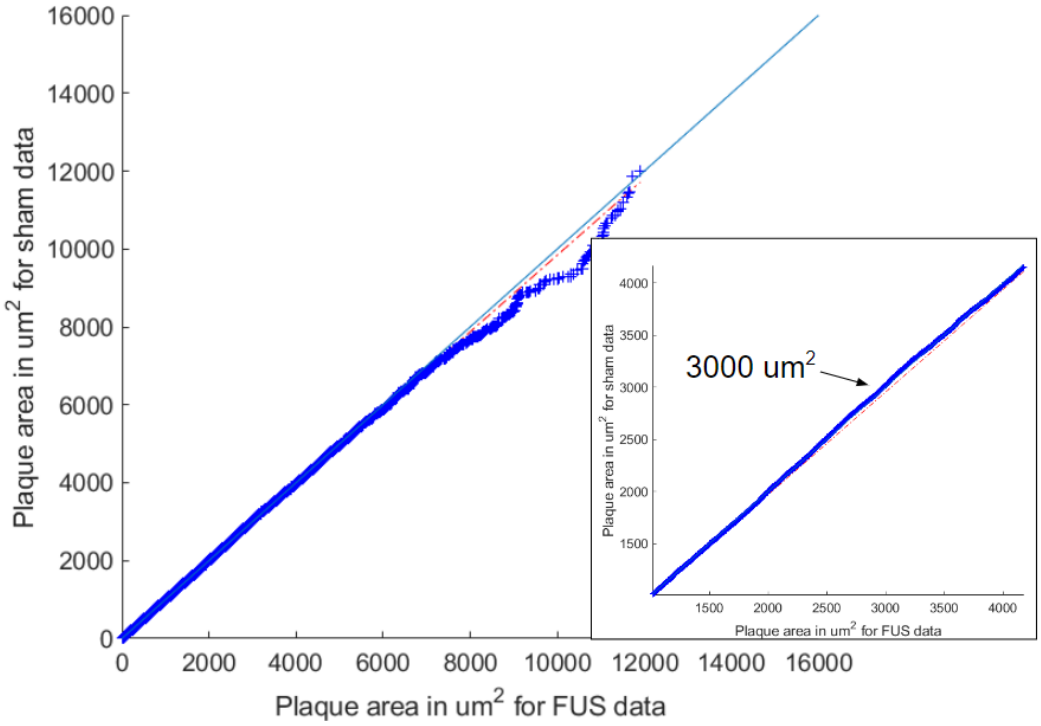

Figure 8. QQ plot of plaque size after five days of FUS versus sham FUS treatment of old AD mice.

This motivated sub-analysis of plaque burden and co-localization at those ranges. The amount of brain covered by plaque of all sizes colocalized with active microglia in mice treated with actual versus sham FUS showed no statistically significant difference (Figures 9, 10), in contrast to what we observed for the young AD mice. This result did not depend upon the cut-off value for plaque area (3000μm²) – results not shown.

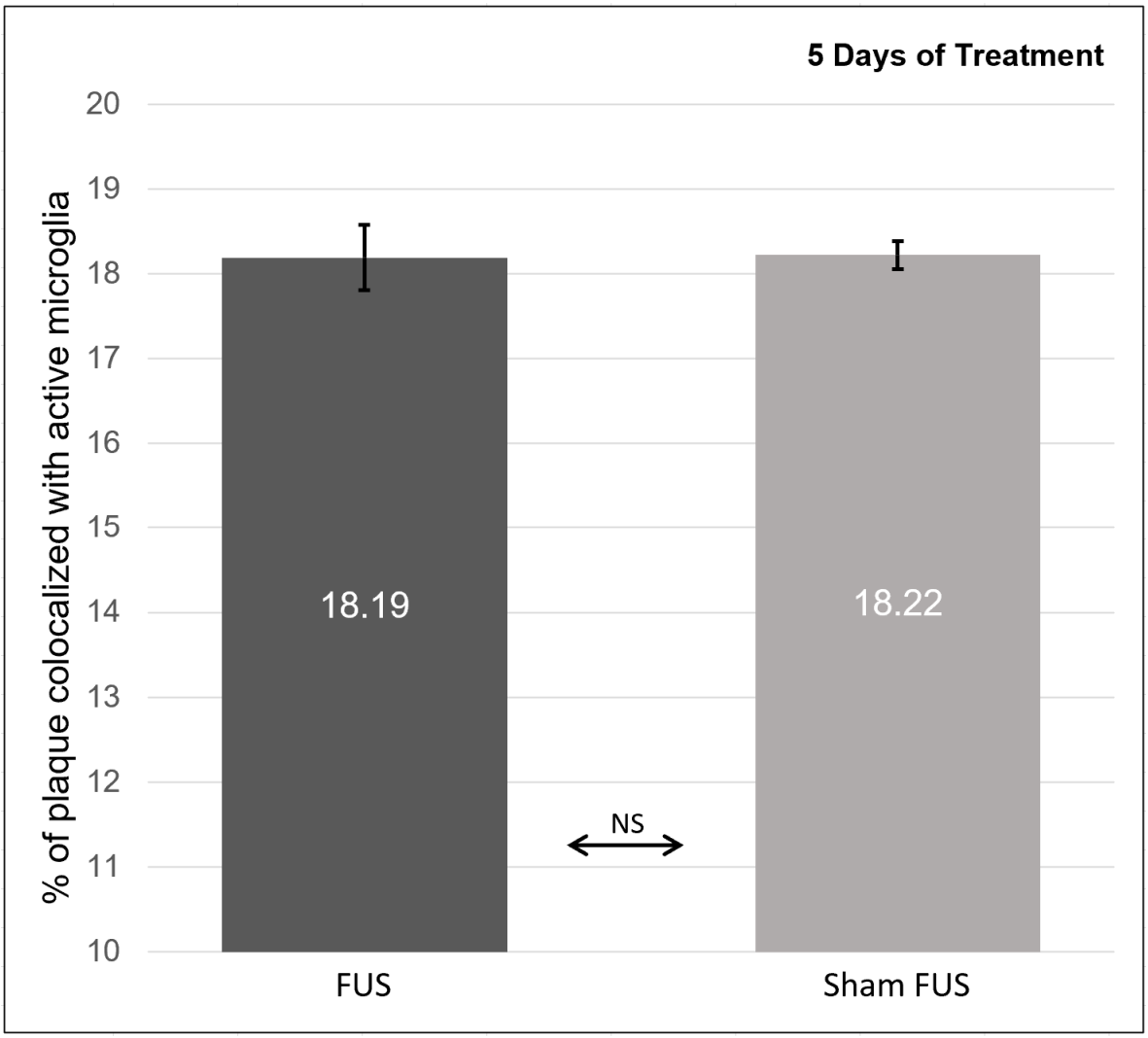

Figure 9. Colocalization of plaque with at least one active microglia in old AD mice (sham) treated with 5 days of FUS. P value of Welch two-sample t-test = 0.86. n = 3 mice with two samples per mouse.

Sham versus actual FUS treatment did not change the plaque burden of these older mice (Figure 10).

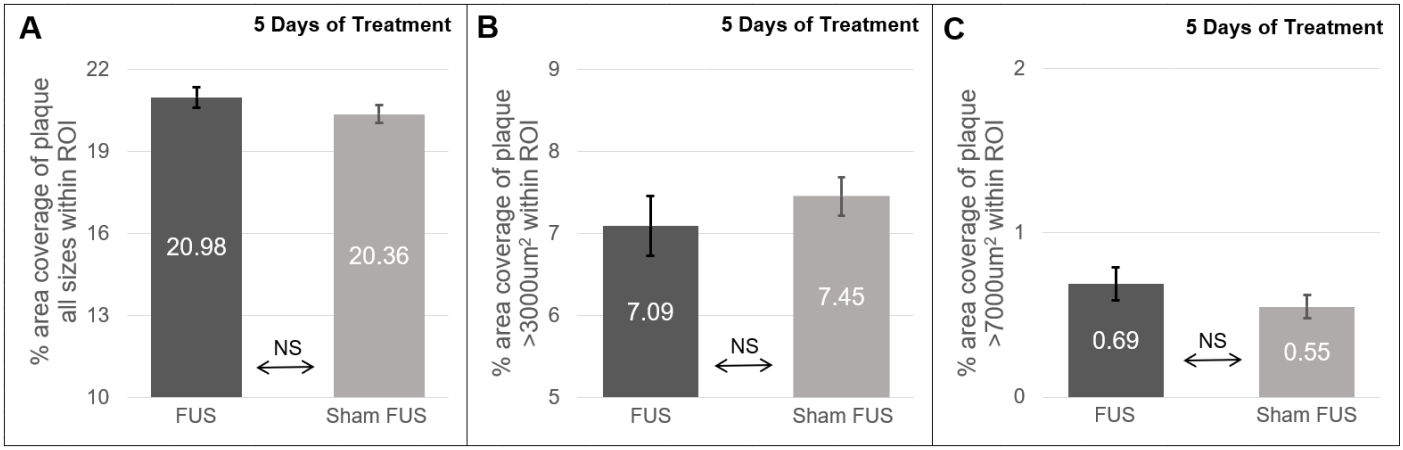

Figure 10. Plaque burden of plaque in different size ranges for old AD mice (sham) treated with 5 days of FUS. **(A)** For percent area of brain covered by plaque of all sizes, Welch two sample t test p value = 0.93. **(B)** For percent area of brain covered by plaque greater than 3000 μm², p value = 0.93. **(C)** For percent area covered by plaque greater than 7000 μm², p value = 0.78. n = 3 mice with two histological samples per mouse.

In contrast to what we observed for the young AD mice, however, the older AD mice treated with FUS had less total eNOS than did untreated AD mice (Fig. 11). Also, the population of eNOS outside of neuronal nuclei was significantly less in mice treated with FUS as compared to sham treatment (Fig. 11). Interestingly, however, and unexpectedly, the distribution of eNOS within neuronal nuclei was significantly greater for mice treated with FUS than with sham FUS.

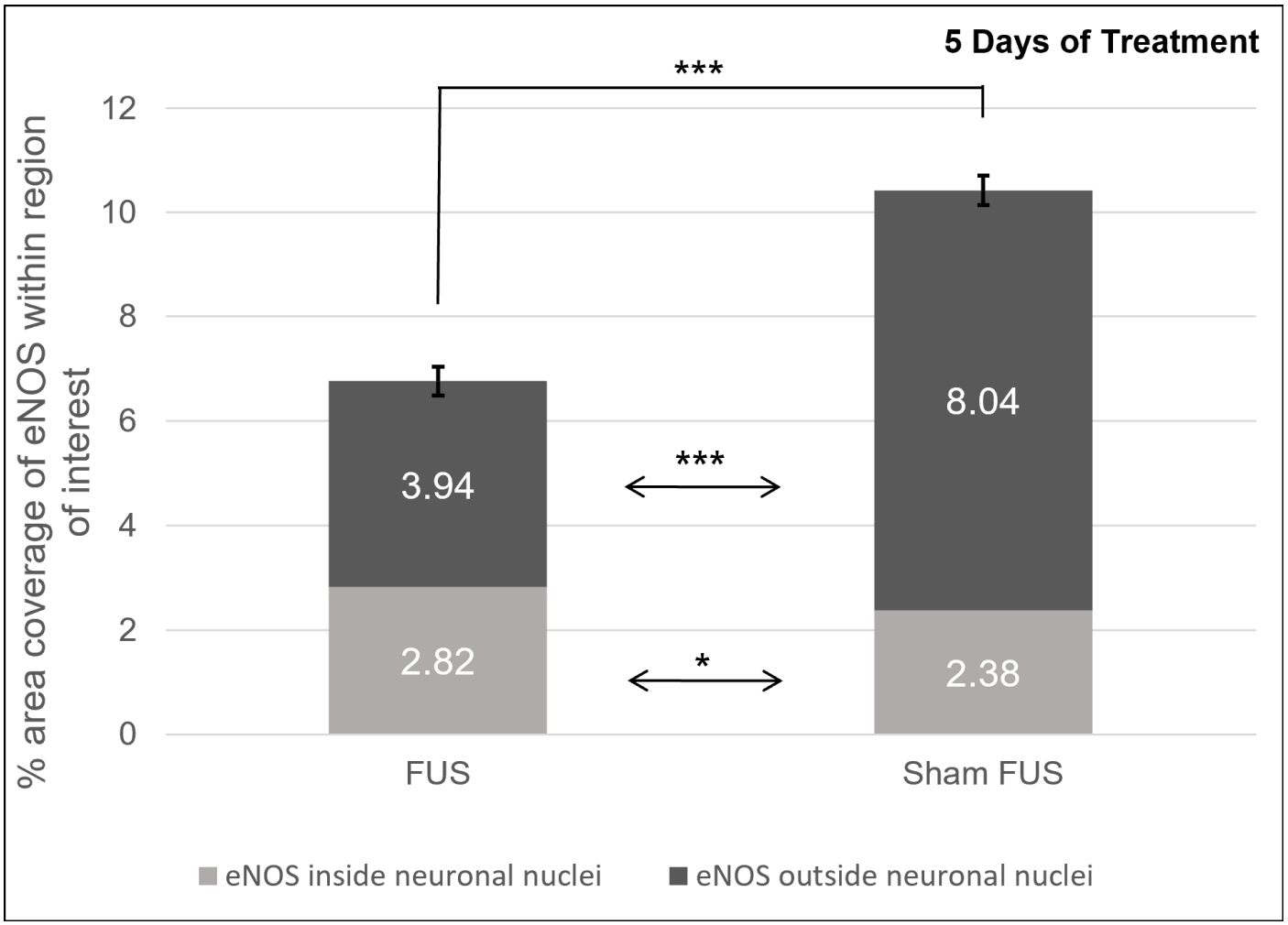

Figure 11. Distribution of eNOS within brain ROI of old AD mice (sham) treated for five days with FUS. Dark gray indicates percentage of brain area coverage of eNOS outside of neuronal nuclei. Light gray indicates eNOS inside neuronal nuclei. p-value of Welch two-sample t-test = 1.28E-04 comparing percent eNOS outside neuronal nuclei. p-value of Welch two-sample t-test = 1.87E-04 comparing percent eNOS inside neuronal nuclei. A p-value for total percent area of brain coverage of eNOS between groups = 0.001. n = 3 mice with two histological samples per mouse.

Table 2. Comparison of 'old' AD mice treated for five days with (sham) FUS. Here, * indicates $p < 0.01$ while *** indicates $p < 0.001$.

Five days of treatment (n = 3 per group) (median +/- SE) Age 12.17 +/- 0.13 (months)			
Parameter	**FUS**		**Sham FUS**
% plaque burden	20.98 +/- 0.75		20.35 +/- 0.67
# of microglia/um^2	0.05 +/- 0.03		0.05 +/- 0.01
# activated microglia/um^2	0.03 +/- 0.03		0.03 +/- 0.03
% colocalized plaque	18.19 +/- 0.78		18.22 +/- 0.33
% area eNOS	6.73 +/- 0.31	***	10.14 +/- 0.59
% eNOS outside neuronal nuclei	64.63 +/- 0.99	***	80.30 +/- 1.89
% eNOS inside neuronal nuclei	35.50 +/- 0.99	*	19.89 +/- 1.91

Table 3 compares results for the three-day and five-day cohorts.

Table 3. Comparison of phenotypic values and associated treatment values for mice treated for three days and five days in relation to age. All quantities except microglia count reported as percentage of the area of ROI. Microglia count is reported as the number of microglia per μm².

	Three days of treatment (n = 3 per group) (median +/- SE)		**Five days of treatment** (n = 3 per group) (median +/- SE)	
Age (months)	7.5 +/- 0.51		12.17 +/- 0.13	
Parameter	**FUS**	**Sham FUS**	**FUS**	**Sham FUS**
% plaque burden	6.10 +/- 1.09	11.25 +/- 2.04	20.98 +/- 0.75	20.35 +/- 0.67
% colocalized plaque	60.08 +/- 3.02	52.17 +/- 3.96	18.19 +/- 0.78	18.22 +/- 0.33
# of microglia/um²	0.18 +/- 0.07	0.15 +/- 0.11	0.05 +/- 0.03	0.05 +/- 0.01
# activated microglia/um²	0.10 +/- 0.10	0.09 +/- 0.09	0.03 +/- 0.03	0.03 +/- 0.03
% area eNOS	2.89 +/- 1.07	3.71 +/- 1.03	6.73 +/- 0.31	10.14 +/- 0.59
% eNOS outside neuronal nuclei	90.16 +/- 4.77	89.63 +/- 1.27	64.63 +/- 0.99	80.30 +/- 1.89
% eNOS inside neuronal nuclei	9.84 +/- 4.77	10.37 +/- 1.27	35.50 +/- 0.99	19.89 +/- 1.91

4. Discussion

Various combinations of vascular inadequacy and buildup of aberrant protein burdens occurs within approximately 75% of dementia cases. A FUS protocol for one hour over five days as used by Bobola et al [21] reduced Aβ burden in 5XFAD mice by ~50%. A different FUS protocol for one hour/day, three days per week, for three months by Eguchi et al [23] et al reduced the Aβ burden using the same mouse model (~15%) while significantly increasing cerebrovascular flow in the same mouse model (by 50%). Taken together, these observations motivated our construction of a novel FUS protocol that combined the protocols of each of Bobola et al [21] and Eguchi et al [23] – Figure 1. In this way we hoped to produce a combination of the two effects, tested here *in vivo*:

Regarding Aβ plaque distribution. Our results show that three days of our combination FUS protocol applied to young mice activated their microglia such that they colocalized with plaque, relative to sham treatment. We also observed a net decrease in Aβ plaque burden for plaque sizes above 1800 μm², with a trend towards reduction of total plaque burden, all relative to sham, relative to sham treatment. In contrast, increasing the treatment to five days and applying the same protocol to significantly older 5XFAD mice did not meaningfully activate microglia nor did it reduce Aβ plaque burden, all relative to sham treatment. **Table 3 summarizes the phenotypic differences in observed brain histology between the young versus old mice that we studied, both for sham and for treated cohorts. The older sham mice (12.2 months old) had a** nearly **twofold *increase* in plaque relative to the younger sham mice (7.5 months old), consistent with the observation of others [**24, 25**]. The older mice also demonstrated a three-fold *decrease* in total microglia relative to the younger mice.** Therefore, there were only a relatively small number of microglia available for activation by FUS hence available to co-localize with a larger amount of plaque in the older versus younger mice. In essence, for the older mice there simply were not enough microglia available to activate via FUS and successfully reduce the Aβ burden, not true for the younger mice.

Regarding eNOS distribution. We differentiated between extra- and intra-neuronal eNOS distributions, unlike Eguchi et al [23], who showed that more *total* eNOS increased net cerebrovascular flow in a causal and functionally consequential way. Without treatment, the percentage of total eNOS within neuronal nuclei nearly doubled from younger to older mice while the percentage of total eNOS associated with extra-neuronal eNOS decreased by 10% from younger to older mice. FUS treatment of younger mice did not alter their total nor partitioned eNOS burden but did so in older 5XFAD mice, for which we observed a reduction in total eNOS and extra-neuronal eNOS along with an increase in intra-neural / intra-nuclear eNOS. The reduction of extra-neuronal eNOS is the opposite of what we intended. The results of Eguchi et al [23] suggests that a reduction of extra-neuronal eNOS by our novel ultrasound protocol would decrease rather than increase cerebral blood flow relative to sham treatment, thereby exacerbating vascular dementia's ischemic effect. Interestingly, however, Li et al [30] demonstrated that intra-neuronal eNOS overexpression can protect against ischemic injury by enhancing BDNF secretion by the neurons, thereby reducing apoptosis and supporting synaptic plasticity. Quoting from their paper: "Our findings suggest that eNOS expressed by neurons functions as a transducer of survival signals, which is upregulated and activated by ischemic stimulation." Thus, the effects of observed increase in intra-neuronal eNOS generated by our FUS protocol may at least partially mitigate the effects of reduced extra-neuronal eNOS also generated by our FUS protocol. Future research that simultaneously assays synaptic function and cerebrovascular flow can test this hypothesis.

That our results depend on the age of the mice highlights an important issue for translation of FUS-based methods of reducing the Aβ burden associated with progressing Alzheimer's Disease. As people age, their Aβ burden increases substantially [31]. Mouse-based studies of FUS for treating AD (and aging in general) should ensure the use of sufficiently aged mice – those known to have representative levels of brain-tissue pathology and brain dysfunction, as have Götz and colleagues [32], for example. In addition, recall the human results of Nicodemus et al [20] – who along with Eguchi et al [23] showed changes in cerebrovascular flow created by ultrasound – and mouse-based studies showing FUS-induced changes in synaptic function as reviewed in Balbi et al [19]. Future *in vivo* and human studies should therefore look beyond changes in aberrant protein burden generated by FUS – and do so in appropriately aged recipients of FUS - to fully appreciate its possible therapeutic effects.

5. Limitations

Our original power analysis, based on our earlier published work, supported our use of n = 3 mice. We did not achieve the same results, however. Future studies with more mice may facilitate demonstration of more differences in the effect of FUS on plaque burden and eNOS distribution versus age than we observed. Likely also important would be increasing the FUS intensity – we chose a value less than half of that of Bobola et al [21] while unpublished research suggests that there may exist a dose response with regard to FUS-mediated activation or inhibition of brain function.

Auditory stimulation by LIFU can activate brain along with, or possibly, instead of direct activation of neurons by FUS energy effects [33]. We did not check for auditory effects in the present study because we relied upon our previous research in the same laboratory for which we determined that there were no auditory differences between sham and treated conditions (Bobola et al, [21]).

6. **Conclusions**

Alzheimer's Disease and vascular dementia contribute up to the majority of dementia cases; AD arises in part due to the buildup of and associated damage created by aberrant proteins (Aβ, tau); vascular dementia results in reduced cerebral blood flow, hence ischemic damage. Our results demonstrate that phenotypical differences in the distribution of microglia and Aβ plaque as a function of age plays an important role in the ability of FUS to activate the former in order to help clear the latter. Our results also show that FUS can manipulate intra-neuronal as well as extra-neuronal processes – here eNOS distribution – with thus-far unknown countervailing effects.

Author Contributions: Conceptualization, AP, KAC, PDM; methodology AP, KAC, PDM; software, AP, KAC; validation, AP, KAC; formal analysis, AP, KAC, PDM; investigation, AP, KAC, HM, JK, HT, GK; resources, AP, KAC, HM, JK, HT, GK; data curation, AP, KAC, HM, JK, HT, GK; writing AP, KAC, PDM; visualization, AP, KAC; supervision, PDM; project administration, PDM; funding acquisition, PDM. All authors have read and agreed to the published version of the manuscript.

Funding: This research was funded by Congressionally Directed Medical Research Programs (CDMRP), grant number W81XWH-20-1-0479.

Institutional Review Board Statement: All animal procedures were approved by the University of Washington Institutional Animal Care and Use Committee under protocol 4084-08 and conformed to applicable national guidelines. This study was approved May 15th, 2019.

Data Availability Statement: Original data available upon reasonable request to the corresponding author (doumitt@uw.edu)

Conflicts of Interest: The authors declare no conflicts of interest.

References

1. Aranda, M. P., Kremer, I. N., Hinton, L., Zissimopoulos, J., Whitmer, R. A., Hummel, C. H., Trejo, L., & Fabius, C. (2021). Impact of dementia: Health disparities, population trends, care interventions, and economic costs. Journal of the American Geriatrics Society, 69(7), 1774–1783. https://doi.org/10.1111/jgs.17345

2. Thal, D. R., Rub, U., Orantes, M., & Braak, H. (2002). Phases of AB-deposition in the human brain and its relevance for the development of ad. Neurology, 58(12), 1791–1800. https://doi.org/10.1212/wnl.58.12.1791

3. Hyman, B. T., Phelps, C. H., Beach, T. G., Bigio, E. H., Cairns, N. J., Carrillo, M. C., Dickson, D. W., Duyckaerts, C., Frosch, M. P., Masliah, E., Mirra, S. S., Nelson, P. T., Schneider, J. A., Thal, D. R., Thies, B., Trojanowski, J. Q., Vinters, H. V., & Montine, T. J. (2012). National Institute on Aging-Alzheimer's Association guidelines for the neuropathologic assessment of Alzheimer's disease. Alzheimer's & dementia : the journal of the Alzheimer's Association, 8(1), 1–13. https://doi.org/10.1016/j.jalz.2011.10.007

4. Montine, T. J., Phelps, C. H., Beach, T. G., Bigio, E. H., Cairns, N. J., Dickson, D. W., Duyckaerts, C., Frosch, M. P., Masliah, E., Mirra, S. S., Nelson, P. T., Schneider, J. A., Thal, D. R., Trojanowski, J. Q., Vinters, H. V., Hyman, B. T., National Institute on Aging, & Alzheimer's Association (2012). National Institute on Aging-Alzheimer's Association guidelines for the neuropathologic assessment of Alzheimer's disease: a practical approach. Acta neuropathologica, 123(1), 1–11. https://doi.org/10.1007/s00401-011-0910-3

5. Masters, C. L., Bateman, R., Blennow, K., Rowe, C. C., Sperling, R. A., & Cummings, J. L. (2015). Alzheimer's disease. Nature reviews. Disease primers, 1, 15056. https://doi.org/10.1038/nrdp.2015.56

6. Jorfi, M., Maaser-Hecker, A., & Tanzi, R. E. (2023). The neuroimmune axis of Alzheimer's disease. Genome medicine, 15(1), 6. https://doi.org/10.1186/s13073-023-01155-w

7. Chakroborty, S., Kim, J., Schneider, C., West, A. R., & Stutzmann, G. E. (2015). Nitric oxide signaling is recruited as a compensatory mechanism for sustaining synaptic plasticity in Alzheimer's disease mice. The Journal of neuroscience : the official journal of the Society for Neuroscience, 35(17), 6893–6902. https://doi.org/10.1523/JNEUROSCI.4002-14.2015

8. Yuste, J. E., Tarragon, E., Campuzano, C. M., & Ros-Bernal, F. (2015). Implications of glial nitric oxide in neurodegenerative diseases. Frontiers in cellular neuroscience, 9, 322. https://doi.org/10.3389/fncel.2015.00322

9. Fleszar, M. G., Wiśniewski, J., Zboch, M., Diakowska, D., Gamian, A., & Krzystek-Korpacka, M. (2019). Targeted metabolomic analysis of nitric oxide/L-arginine pathway metabolites in dementia: association with pathology, severity, and structural brain changes. Scientific reports, 9(1), 13764. https://doi.org/10.1038/s41598-019-50205-0

10. Beshir, S. A., Aadithsoorya, A. M., Parveen, A., Goh, S. S. L., Hussain, N., & Menon, V. B. (2022). Aducanumab Therapy to Treat Alzheimer's Disease: A Narrative Review. International journal of Alzheimer's disease, 2022, 9343514. https://doi.org/10.1155/2022/9343514

11. Iaccarino, H. F., Singer, A. C., Martorell, A. J., Rudenko, A., Gao, F., Gillingham, T. Z., Mathys, H., Seo, J., Kritskiy, O., Abdurrob, F., Adaikkan, C., Canter, R. G., Rueda, R., Brown, E. N., Boyden, E. S., & Tsai, L. H. (2016). Gamma frequency entrainment attenuates amyloid load and modifies microglia. Nature, 540(7632), 230–235. https://doi.org/10.1038/nature20587

12. Martorell, A. J., Paulson, A. L., Suk, H. J., Abdurrob, F., Drummond, G. T., Guan, W., Young, J. Z., Kim, D. N., Kritskiy, O., Barker, S. J., Mangena, V., Prince, S. M., Brown, E. N., Chung, K., Boyden, E. S., Singer, A. C., & Tsai, L. H. (2019). Multi-sensory Gamma Stimulation Ameliorates Alzheimer's-Associated Pathology and Improves Cognition. Cell, 177(2), 256–271.e22. https://doi.org/10.1016/j.cell.2019.02.014

13. Chan, D., Suk, H. J., Jackson, B. L., Milman, N. P., Stark, D., Klerman, E. B., Kitchener, E., Fernandez Avalos, V. S., de Weck, G., Banerjee, A., Beach, S. D., Blanchard, J., Stearns, C., Boes, A. D., Uitermarkt, B., Gander, P., Howard, M., 3rd, Sternberg, E. J., Nieto-Castanon, A., Anteraper, S., … Tsai, L. H. (2022). Gamma frequency sensory stimulation in mild probable Alzheimer's dementia patients: Results of feasibility and pilot studies. PloS one, 17(12), e0278412. https://doi.org/10.1371/journal.pone.0278412

14. Leinenga G, Götz J. Scanning ultrasound removes amyloid-β and restores memory in an Alzheimer's disease mouse model. Sci Transl Med. 2015 Mar 11;7(278):278ra33. Doi: 10.1126/scitranslmed.aaa2512.

15. Karakatsani ME, Ji R, Murillo MF, Kugelman T, Kwon N, Lao YH, Liu K, Pouliopoulos AN, Honig LS, Duff KE, Konofagou EE. Focused ultrasound mitigates pathology and improves spatial memory in Alzheimer's mice and patients. Theranostics. 2023 Jul 14;13(12):4102-4120. Doi: 10.7150/thno.79898.

16. Rezai AR, D'Haese PF, Finomore V, Carpenter J, Ranjan M, Wilhelmsen K, Mehta RI, Wang P, Najib U, Vieira Ligo Teixeira C, Arsiwala T, Tarabishy A, Tirumalai P, Claassen DO, Hodder S, Haut MW. Ultrasound Blood-Brain Barrier Opening and Aducanumab in Alzheimer's Disease. N Engl J Med. 2024 Jan 4;390(1):55-62. Doi: 10.1056/NEJMoa2308719.

17. Mehta RI, Ranjan M, Haut MW, Carpenter JS, Rezai AR. Focused Ultrasound for Neurodegenerative Diseases. Magn Reson Imaging Clin N Am. 2024 Nov;32(4):681-698. doi: 10.1016/j.mric.2024.03.001. Epub 2024 Jul 26.

18. Leinenga G, Koh WK, Götz J. Scanning ultrasound in the absence of blood-brain barrier opening is not sufficient to clear β-amyloid plaques in the APP23 mouse model of Alzheimer's disease. Brain Res Bull. 2019 Nov;153:8-14. Doi: 10.1016/j.brainresbull.2019.08.002. Epub 2019 Aug 7.

19. Balbi M, Blackmore DG, Padmanabhan P, Götz J. Ultrasound-Mediated Bioeffects in Senescent Mice and Alzheimer's Mouse Models. Brain Sci. 2022 Jun 13;12(6):775. Doi: 10.3390/brainsci12060775.

20. Nicodemus NE, Becerra S, Kuhn TP, Packham HR, Duncan J, Mahdavi K, Iovine J, Kesari S, Pereles S, Whitney M, Mamoun M, Franc D, Bystritsky A, Jordan S. Focused transcranial ultrasound for treatment of neurodegenerative dementia. Alzheimers Dement (N Y). 2019 Aug 8;5:374-381. doi: 10.1016/j.trci.2019.06.007.

21. Bobola, M. S., Chen, L., Ezeokeke, C. K., Olmstead, T. A., Nguyen, C., Sahota, A., Williams, R. G., & Mourad, P. D. (2020). Transcranial focused ultrasound, pulsed at 40 Hz, activates microglia acutely and reduces Aβ load chronically, as demonstrated in vivo. Brain stimulation, 13(4), 1014–1023. https://doi.org/10.1016/j.brs.2020.03.016

22. Park M, Hoang GM, Nguyen T, Lee E, Jung HJ, Choe Y, Lee MH, Hwang JY, Kim JG, Kim T. Effects of transcranial ultrasound stimulation pulsed at 40 Hz on Aβ plaques and brain rhythms in 5×FAD mice. Transl Neurodegener. 2021 Dec 7;10(1):48. doi: 10.1186/s40035-021-00274-x. PMID: 34872618; PMCID: PMC8650290.

23. Eguchi K, Shindo T, Ito K, Ogata T, Kurosawa R, Kagaya Y, Monma Y, Ichijo S, Kasukabe S, Miyata S, Yoshikawa T, Yanai K, Taki H, Kanai H, Osumi N, Shimokawa H. Whole-brain low-intensity pulsed ultrasound therapy markedly improves cognitive dysfunctions in mouse models of dementia - Crucial roles of endothelial nitric oxide synthase. Brain Stimul. 2018 Sep-Oct;11(5):959-973. doi: 10.1016/j.brs.2018.05.012. Epub 2018 May 22. PMID: 29857968.

24. Oblak, A. L., Lin, P. B., Kotredes, K. P., Pandey, R. S., Garceau, D., Williams, H. M., Uyar, A., O'Rourke, R., O'Rourke, S., Ingraham, C., Bednarczyk, D., Belanger, M., Cope, Z. A., Little, G. J., Williams, S. G., Ash, C., Bleckert, A., Ragan, T., Logsdon, B. A., Mangravite, L. M., … Lamb, B. T. (2021). Comprehensive Evaluation of the 5XFAD Mouse Model for Preclinical Testing Applications: A MODEL-AD Study. Frontiers in aging neuroscience, 13, 713726. https://doi.org/10.3389/fnagi.2021.713726

25. Mar KD, So C, Hou Y, Kim JC. Age dependent path integration deficit in 5xFAD mice. Behav Brain Res. 2024 Apr 12;463:114919. doi: 10.1016/j.bbr.2024.114919. Epub 2024 Feb 24.

26. Faul F, Erdfelder E, Lang AG, Buchner A. G*Power 3: a flexible statistical power analysis program for the social, behavioral, and biomedical sciences. Behav Res Methods. 2007 May;39(2):175-91. doi: 10.3758/bf03193146.

27. Devore JL, Farnum NR, Doi JA (2014) Applied statistics for engineers and scientists. 3rd edition. Cengage Learning, Stamford CT 06902

28. Das, S., & Ramanan, N. (2023). Region-specific heterogeneity in neuronal nuclear morphology in young, aged and in Alzheimer's disease mouse brains. Frontiers in cell and developmental biology, 11, 1032504. https://doi.org/10.3389/fcell.2023.1032504

29. Caviedes, A., Varas-Godoy, M., Lafourcade, C., Sandoval, S., Bravo-Alegria, J., Kaehne, T., Massmann, A., Figueroa, J. P., Nualart, F., & Wyneken, U. (2017). Endothelial nitric oxide synthase is present in dendritic spines of neurons in primary cultures. Frontiers in Cellular Neuroscience, 11. https://doi.org/10.3389/fncel.2017.00180

30. Li ST, Pan J, Hua XM, Liu H, Shen S, Liu JF, Li B, Tao BB, Ge XL, Wang XH, Shi JH, Wang XQ. Endothelial nitric oxide synthase protects neurons against ischemic injury through regulation of brain-derived neurotrophic factor expression. CNS Neurosci Ther. 2014 Feb;20(2):154-64. doi: 10.1111/cns.12182. Epub 2014 Jan 8.

31. Braak H, Thal DR, Ghebremedhin E, Del Tredici K. Stages of the pathologic process in Alzheimer disease: age categories from 1 to 100 years. J Neuropathol Exp Neurol. 2011 Nov;70(11):960-9. **D**oi: 10.1097/NEN.0b013e318232a379**.**

32. Götz J, Richter-Stretton G, Cruz E. Therapeutic Ultrasound as a Treatment Modality for Physiological and Pathological Ageing Including Alzheimer's Disease. Pharmaceutics. 2021 Jul 1;13(7):1002. doi: 10.3390/pharmaceutics13071002.

33. Guo H, Hamilton M 2nd, Offutt SJ, Gloeckner CD, Li T, Kim Y, Legon W, Alford JK, Lim HH. Ultrasound Produces Extensive Brain Activation via a Cochlear Pathway. Neuron. 2018 Jun 6;98(5):1020-1030.e4. doi: 10.1016/j.neuron.2018.04.036. Epub 2018 May 24. Erratum in: Neuron. 2018 Aug 22;99(4):866. **D**oi: 10.1016/j.neuron.2018.07.049.